Charged-particle chaotic dynamics in rotational discontinuities

Francesco Malara,* Silvia Perri,† and Gaetano Zimbardo‡
Dipartimento di Fisica, Università della Calabria, Ponte P. Bucci, cubo 31 C, 87036 Rende (CS), Italy

(Received 20 April 2021; accepted 2 August 2021; published 24 August 2021)

The interplanetary plasma is characterized by a high level of complexity over a broad range of spatial scales. Spacecraft have detected a large variety of embedded structures that have been identified as discontinuities in the magnetic field vector. They can be either generated within the solar corona and advected by the plasma flow or locally generated as a result of the turbulent cascade of the solar wind turbulence. Since magnetic field fluctuations and structures influence the energetic particle propagation, here we set up a numerical model to study the interaction between charged particles and an ideal magnetohydrodynamics rotational discontinuity. This interaction is strongly influenced by the model parameters, such as the rotation angle of the discontinuity, the orientation of the mean-field direction with respect to the normal to the discontinuity direction, the initial particle pitch angle, and the initial particle gyrophase. Numerical results clearly show that the motion of particles crossing the discontinuity is extremely complex and highly sensitive to the initial conditions of the system, with transitions to a chaotic behavior. We find that particles can be temporarily trapped in rotational discontinuity and that the trapping times have a nearly power-law distribution. Also, the separatrix in the initial conditions phase space between crossing and noncrossing trajectories has a fractal structure. Implications for energetic particle propagation in space plasmas are discussed.

DOI: 10.1103/PhysRevE.104.025208

I. INTRODUCTION

A crucial and still open problem in astrophysics is the transport of energetic particles in the heliosphere and in the interstellar medium. In the heliosphere, even in the surroundings of the Earth, energetic particles with a wide spectrum of energies, ranging from a few tens of keV up to $\leqslant 1$ GeV are frequently observed [1]. These particles can be accelerated by flares in the solar corona and by coronal mass ejections (solar energetic particles), and by interplanetary shocks. Their transport properties are strictly related to magnetic turbulence [2,3] and to coherent structures [4], that are ubiquitously present in astrophysical plasmas [5–7]. Pitch-angle diffusion, connected with transport in the direction parallel to magnetic field, drift motions due to magnetic field inhomogeneities, as well as transverse diffusion due to random walk of magnetic lines are all aspects of energetic particle transport that are controlled by magnetic turbulence properties, such as fluctuation amplitude, spectral index and anisotropy [2,3,8–10]. In addition, how particles interact with structures, waves, and fluctuations has fundamental implications for particle acceleration processes at interplanetary shock waves, since fast pitch-angle diffusion, as well as slow spatial diffusion, can speed up the acceleration process [11–14].

A number of studies show that turbulence cannot be simply considered as a superposition of random fluctuations at different spatial scales. In fact, a relevant aspect is the presence of coherent structures that dynamically form in the turbulent cascade process toward small scales [15–18]. Examples are current sheets, tangential (TDs) or rotational discontinuities (RDs), routinely observed in the solar wind turbulence [19–22]. Such structures have also been detected in the inner heliosphere by Parker Solar Probe [23]. RDs will have a *nontrivial* influence (distinct from fluid effects) on energetic particles whose gyroradius is comparable to the thickness of the RD, which in the solar wind can be estimated as of the order of 10^4 km (see details below). This may correspond to energies in the range from 100 keV to 1 MeV. However, the effect of RDs or TDs on particle transport has scarcely been investigated in the literature. Since these structures have the potential to cause fast, large pitch-angle scattering, it is crucial to understand their effects on particle motion. A recent work describing the interaction of ions with a RD, based on the Hamiltonian formalism, has shown that fast pitch-angle scattering is indeed possible, and that it is related to the destruction of the longitudinal adiabatic invariant due to separatrix crossing in phase space [24].

The magnetic field $\mathbf{B}$ has a rotation when crossing either a RD or a TDs. In the framework of magnetohydrodynamics (MHD), RDs are planar structures that have a nonvanishing, constant magnetic field component B_n in the normal direction [in a one-dimensional (1D) model, $\nabla \cdot \mathbf{B} = 0$ implies that B_n is constant], while pressure and magnetic field intensity are continuous across the discontinuity. Moreover, RDs propagate at the Alfvén speed $v_A = B_n/(4\pi\rho)^{1/2}$ (with ρ the mass density) along the mean magnetic field. TDs have vanishing B_n and can have arbitrary jumps in plasma and magnetic pressure, though the total pressure remains constant across the discontinuity. TDs do not propagate in the plasma reference frame

*francesco.malara@fis.unical.it
†silvia.perri@fis.unical.it
‡gaetano.zimbardo@fis.unical.it

and can be interpreted as the boundary between two adiacent magnetic flux tubes [25]. In the limit $B_n \to 0$, a RD becomes a TD where plasma and magnetic pressure are constant across the discontinuity.

In single-spacecraft studies the variance matrix method has been applied to discriminate between RDs and TDs [19,26–31]. In most cases, either RDs or TDs have been found to be prevalent in fast-speed or in slow-speed streams, respectively. Other studies based on multispacecraft observations [32–35] have found a dominance of cases with large $\theta_{\rm Bn}$ (the largest angle between the upstream or downstream magnetic field and the normal direction) and small $\Delta B/B$, which can be interpreted either as RDs propagating at a large angle with respect to the ambient magnetic field, or as TDs with a small jump in the magnetic intensity [34,35]. The presence of RDs in fast-speed streams seems to be related with quasi-uniform-intensity magnetic field fluctuations that characterize such streams [36]; this relationship has independently been found by Roberts [37] and by Valentini *et al.* [38] using different methods.

The present paper deals with some aspect of the energetic particle dynamics in the presence of such discontinuities. We investigate by numerical simulations the dynamics of high-energy charged particles when encountering a RD. The latter is described by a constant $|\mathbf{B}|$ analytical model. Our purpose is to single out the role of RDs in pitch-angle scattering, by studying how the pitch angle is modified when a particle crosses a RD, for different configurations of the RD.

The plan of the paper is the following: in Secs II and III the magnetic field model and particle dynamics setup are respectively described; in Sec. IV numerical results are presented; finally, a discussion and conclusive considerations are given in Sec. V.

II. THE MODEL

A charged particle moving in an electromagnetic field is subject to the Lorentz force $\mathbf{F} = \mathbf{F}_e + \mathbf{F}_m = q\mathbf{E} + q\mathbf{v} \times \mathbf{B}/c$, where $\mathbf{E}$ and $\mathbf{B}$ are the electric and magnetic field, respectively, q and $\mathbf{v}$ are the particle charge and velocity, and c is the speed of light. The relative intensity of the electric to magnetic force F_e/F_m can be estimated by the following argument: Indicating by δE and δB the amplitude of electric and magnetic field fluctuations characterized by spatial and temporal scales ℓ and τ, respectively, the following relation is derived from the Faraday's law: $\delta E \sim (\ell/\tau)(\delta B/c) \sim (v_\phi/c)\delta B$ where v_ϕ is the propagation speed of fluctuations. Assuming that $v_\phi \sim v_A$ with v_A the Alfvén velocity, we obtain

$$\frac{F_e}{F_m} \sim \frac{\delta E}{v\delta B/c} \sim \frac{v_A}{v}. \tag{1}$$

To fix the ideas, we consider high-energy protons with a kinetic energy $\mathcal{E}_p = m_p v^2/2 = 1$ MeV, with m_p the proton mass, therefore moving with a velocity $v_{\rm 1MeV} \simeq 1.38 \times 10^9$ cm/s. This energy is roughly in the middle of the energy range for energetic particles observed in the heliosphere, and corresponds to Larmor radii comparable to the magnetic field line radius of curvature, see Fig. 3. Assuming for the Alfvén speed the value $v_A \sim (3\text{–}5) \times 10^6$ cm/s, typical of the solar wind, from Eq. (1) we obtain $F_e/F_m \sim (2.2\text{–}3.6) \times 10^{-3}$. We conclude that, when describing the dynamics of such particles, we can neglect the contribution of the electric force. For the same reason we neglect the time dependence in the magnetic field $\mathbf{B}$. Therefore, the motion equations can be written in the following dimensionless form:

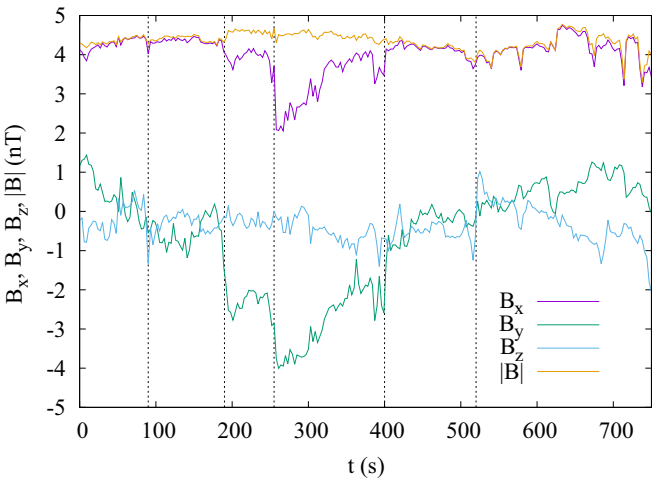

FIG. 1. Magnetic field components B_x, B_y, B_z and intensity $|\mathbf{B}|$, from the dataset of the Wind spacecraft, are plotted as functions of time t. The reference frame is such that the z axis corresponds to the minimum variance direction for the considered sample of data. RDs are present around times $t \simeq 90$ s, $t \simeq 190$ s, $t \simeq 255$ s, $t \simeq 400$ s, and $t \simeq 520$ s (vertical dashed lines).

$$\frac{d\mathbf{v}}{dt} = \mathbf{v} \times \mathbf{B}(\mathbf{r}), \qquad \frac{d\mathbf{r}}{dt} = \mathbf{v}, \tag{2}$$

where the position $\mathbf{r}$ is normalized to a length ℓ that represents the width of the RD; the magnetic field $\mathbf{B}$ is normalized to a typical value B_0, time t is normalized to $1/\Omega_0$, with $\Omega_0 = qB_0/(m_p c)$ the corresponding gyrofrequency, and the velocity $\mathbf{v}$ is normalized to $\tilde{v} = \ell\Omega_0$. To simplify the notation, from now on we indicate dimensionless quantities with the same symbols as the corresponding dimensional quantities. To assess the values of ℓ and B_0 we consider a dataset of magnetic field measurements obtained in a fast-speed stream by the Wind spacecraft. A sample of such dataset is plotted in Fig. 1, where rapid rotations of $\mathbf{B}$, corresponding to RDs, are visible. These structures are actually advected by the solar wind flow with a speed much larger than both the spacecraft speed (which is moving at less than 10^6 cm s^{-1}) and the typical propagation speed (i.e., v_A). Thus, RDs can be considered frozen into the bulk flow. The magnetic field magnitude $|\mathbf{B}|$ has much smaller variations, corresponding to continuous magnetic pressure across RDs. From the magnetic field data, we estimate a typical time the spacecraft takes to cross a RD as $t_{\rm RD} \sim 10$ s; being the solar wind velocity in this interval $v_{\rm SW} \sim 6 \times 10^7$ cm s^{-1} the corresponding RD width is $\ell = v_{\rm SW} t_{\rm RD} \sim 6 \times 10^8$ cm. We estimate a typical value for the magnetic field $B_0 \simeq 4 \times 10^{-5}$ G, corresponding to $\Omega_0 = qB_0/(m_p c) \simeq 0.38$ s^{-1}. This gives $\tilde{v} = \ell\Omega_0 \simeq 2.3 \times 10^8$ cm/s. Therefore, the normalized value for the velocity of 1 MeV protons is $v = v_{\rm 1MeV}/\tilde{v} = 6$.

We consider a form for the magnetic field dependence $\mathbf{B}(\mathbf{r})$ that represents a simple model for a RD. Defining a Cartesian

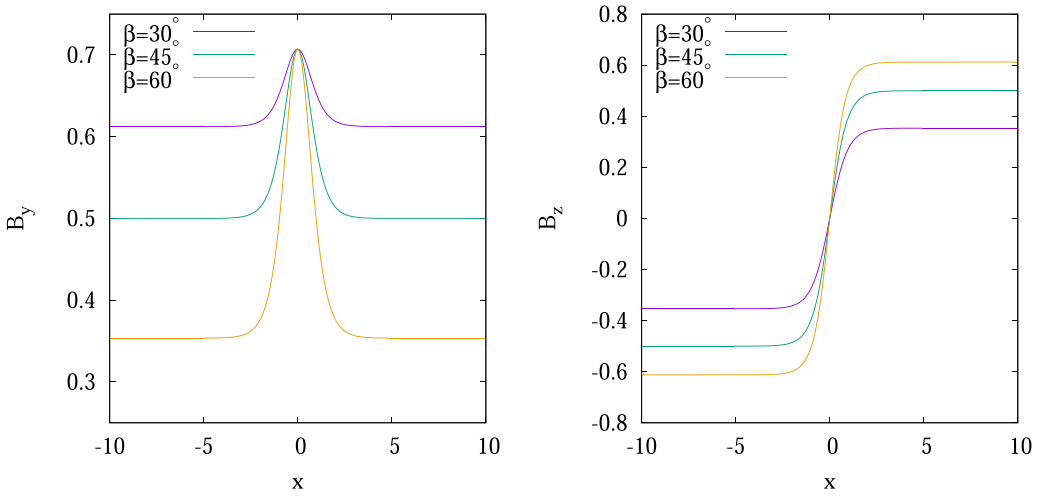

FIG. 2. Magnetic field components B_y (left) and B_z (right), corresponding to the expression (3), are plotted as functions of x, for $\alpha = 45^\circ$ and $\beta = 30^\circ$ (purple lines), $\beta = 45^\circ$ (green lines), and $\beta = 60^\circ$ (orange lines)

reference frame $\{x, y, z\}$, we assume a planar structure where $\mathbf{B}$ depends only on the x coordinate. The conditions $\nabla \cdot \mathbf{B} = 0$ implies that $B_x \equiv B_n = \text{const}$. More explicitly, we assume the following expression:

$$\mathbf{B}(x) = \cos\alpha\, \mathbf{e}_x + \sin\alpha\, \{\cos[\psi(x)]\mathbf{e}_y + \sin[\psi(x)]\mathbf{e}_z\},$$
$$\text{with} \quad \psi(x) = \beta \tanh(x), \tag{3}$$

where α and β are constant angles and $\mathbf{e}_x$, $\mathbf{e}_y$, and $\mathbf{e}_z$ are the unit vectors along the Cartesian axes. The quantity $\psi(x)$ represents the angle between the transverse magnetic field component $\mathbf{B}_T = B_y\mathbf{e}_y + B_z\mathbf{e}_z$ and the y axis. Increasing x from negative to positive values, $\mathbf{B}_T$ rotates by an angle 2β, while the angle α between $\mathbf{B}$ and the normal component $\mathbf{B}_n = \cos\alpha\, \mathbf{e}_x$ remains constant. The width of the RD is $\ell = 1$ and the magnetic field magnitude is uniform $|\mathbf{B}| = 1$, in normalized units. The magnetic field (3) depends only on two parameters, namely, the angles α and β: Larger values of β correspond to a wider rotation of $\mathbf{B}$ across the RD; in the limit $\alpha \to 90^\circ$ the RD tends to a TD with no magnetic pressure jump. Profiles of components B_y and B_z as functions of x are shown in Fig. 2 for $\alpha = 45^\circ$ and different values β.

III. PARTICLE DYNAMICS

Since we neglect the electric field in our model, the kinetic energy is conserved. Therefore, an increase (decrease) of the parallel velocity $v_{||} = (\mathbf{v} \cdot \mathbf{B})/B$ during a particle crossing of the RD corresponds to a decrease (increase) of the perpendicular velocity $v_\perp = |\mathbf{v} - v_{||}\mathbf{B}/B|$ and of the Larmor radius $\rho = v_\perp/B$ (in normalized units). To quantify this phenomenon, we consider the time evolution of the pitch-angle cosine $w(t) = v_{||}(t)/v$, related to the Larmor radius by $\rho = v\sqrt{1-w^2}/B$. We consider particles that at the initial time $t = 0$ are located upstream of the RD, moving toward the RD with a given $w_0 = w(t = 0)$. After interacting with the RD, the particle has a final pitch-angle cosine w_1 that, in general, is different from w_0. In cases when the sign of w_1 is opposite to that of w_0 the particle is reflected back by the RD. In general, the random variation $\Delta w = w_1 - w_0$ in a population of particles can give rise to parallel diffusion.

One can expect a different behavior of particles according to whether the Larmor radius ρ is smaller or larger than the curvature radius R_c of magnetic lines [39]. Indeed, for $\rho \ll R_c$ the conservation of magnetic momentum $\mu = m_p v_\perp^2/(2B)$ is assumed. In our case where $|\mathbf{B}|$ is constant, this implies that also $w(t)$ is (approximately) constant. Therefore, we expect to find significant variations Δw when ρ is of the order of or larger than R_c. The curvature radius is defined by $R_c = |d\hat{\mathbf{b}}/ds|^{-1}$, where $\hat{\mathbf{b}} = \mathbf{B}/B$ and ds is the arc length increment along the magnetic line. In our case $dx = \cos\alpha\, ds$; therefore, $R_c = (\cos\alpha |d\hat{\mathbf{b}}/dx|)^{-1}$. Using the expressions (3), we find $R_c(x) = \cosh^2(x)/(\beta \sin\alpha \cos\alpha)$. The minimum curvature radius is at the center of the RD ($x = 0$):

$$R_{c,\min} = R_c(x = 0) = \frac{1}{\beta \sin\alpha \cos\alpha}. \tag{4}$$

In Fig. 3 the minimum curvature radius $R_{c,\min}$ is plotted as a function of α, for various values of β. The minimum $\min_\alpha\{R_{c,\min}\}$ is found for $\alpha = 45^\circ$ and this quantity decreases for increasing β. For reference, on the same figure we superposed the value $\rho_{\max} = v/B = 6$. Fig. 3 indicates that larger variations $|\Delta w|$ are to be expected for a broad range of values around 45° and for large values of the rotation angle β.

The initial position for all particles is $(x_0, y_0, z_0) = (-30, 0, 0)$. The value $|x_0|$ is sufficiently large to guarantee that the initial position is located outside the RD. The values of y_0 and z_0 are not relevant since $\mathbf{B}$ depends only on x. To define the initial velocity we consider another reference frame $\{x', y', z'\}$, where the z' axes is parallel to $\mathbf{B}(x_0)$. With respect to such a reference frame, the initial velocity is defined as

$$\mathbf{v}_0 = v\big[\sqrt{1-w_0^2}(\cos\phi_0 \mathbf{e}_{x'} + \sin\phi_0 \mathbf{e}_{y'}) + w_0 \mathbf{e}_{z'}\big], \tag{5}$$

where $v = 6$ in normalized units (i.e., $v_{1\text{MeV}} \simeq 1.38 \times 10^9$ cm/s), $0 < w_0 \leqslant 1$, corresponding to particles moving toward the RD, and $\phi_0 \in [0, 2\pi]$ is the initial gyrophase. The unit vector along the z' axis is $\mathbf{e}_{z'} = \mathbf{B}(x_0)/B(x_0)$; the unit vector along the y' axis is chosen to be perpendicular both to

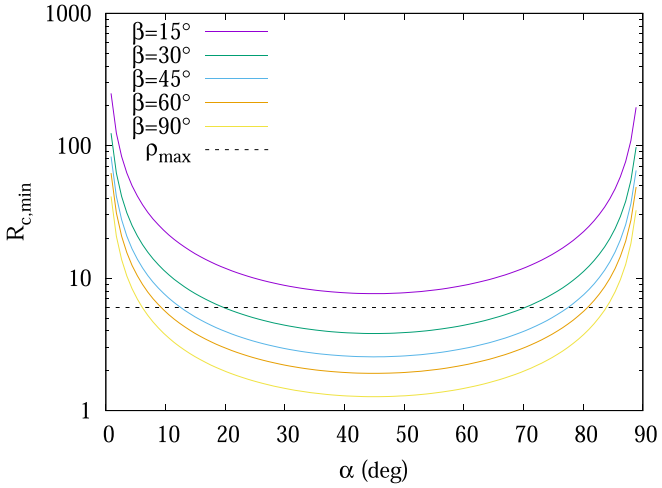

FIG. 3. The minimum curvature radius $R_{c,\min}$ is plotted as a function of α for different values of β: $\beta = 15^\circ$ (purple line), $\beta = 30^\circ$ (green line), $\beta = 45^\circ$ (light blue line), $\beta = 60^\circ$ (orange line), and $\beta = 90^\circ$ (yellow line). The dashed line indicates the value $\rho_{\max} = 6$.

the x axis and to $\mathbf{e}_{z'}$: $\mathbf{e}_{y'} = (\mathbf{e}_x \times \mathbf{e}_{z'})/|\mathbf{e}_x \times \mathbf{e}_{z'}|$; finally, $\mathbf{e}_{x'} = (\mathbf{e}_{y'} \times \mathbf{e}_{z'})/|\mathbf{e}_{y'} \times \mathbf{e}_{z'}|$. A sketch of the geometry is illustrated in Fig. 4: the magnetic field $\mathbf{B}$ at the initial position $x = x_0$, its components B_x and $\mathbf{B}_T$, angles α and $\psi(x_0) = -\beta$ (green elements), the $\{x', y', z'\}$ axes (blue), the initial particle velocity $\mathbf{v}_0$, the initial pitch angle θ_0 and gyrophase ϕ_0 (red elements). Moving along x, the component B_x remains constant while the transverse component $\mathbf{B}_T$ rotates in the yz plane by varying ψ.

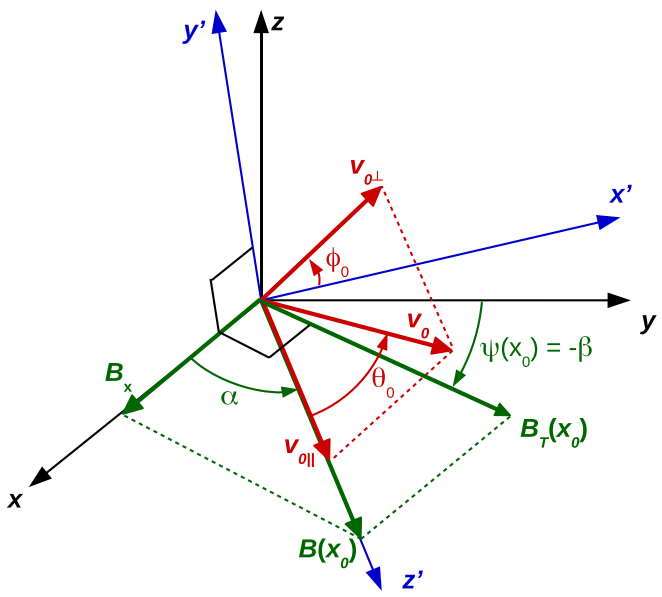

FIG. 4. A sketch of the geometry is illustrated: the magnetic field $\mathbf{B}$ at the initial position $x = x_0$, its components B_x and $\mathbf{B}_T$, angles α and $\psi(x_0) = -\beta$ (green elements), the $\{x', y', z'\}$ axes (blue), the initial particle velocity $\mathbf{v}_0$, the initial pitch angle θ_0, and gyrophase ϕ_0 (red elements). The y' axis and the magnetic field transverse component $\mathbf{B}_T$ are both perpendicular to the x axis, as explicitly indicated.

Using the above definitions, the initial velocity components with respect to the $\{x, y, z\}$ reference frame are given by

$$
\begin{aligned}
v_{0x} &= -\frac{B_y(x_0)}{B(x_0)} v \cos\phi_0 \sqrt{1-w_0^2} + \frac{B_x(x_0)}{B(x_0)} v w_0 \\
v_{0y} &= \frac{B_x(x_0)B_y(x_0)}{B(x_0)B_{yz}(x_0)} v \cos\phi_0 \sqrt{1-w_0^2} \\
&\quad - \frac{B_z(x_0)}{B_{yz}(x_0)} v \sin\phi_0 \sqrt{1-w_0^2} + \frac{B_y(x_0)}{B(x_0)} v w_0 \\
v_{0z} &= \frac{B_x(x_0)B_z(x_0)}{B(x_0)B_{yz}(x_0)} v \cos\phi_0 \sqrt{1-w_0^2} \\
&\quad + \frac{B_y(x_0)}{B_{yz}(x_0)} v \sin\phi_0 \sqrt{1-w_0^2} + \frac{B_z(x_0)}{B(x_0)} v w_0
\end{aligned}
\tag{6}
$$

where $B_{yz} = \sqrt{B_y^2 + B_z^2}$. In expressions (6) we will vary the parameters w_0 and ϕ_0 that define the direction of the initial velocity.

The motion equations (2) are numerically integrated by using the Boris method. It has been shown that this method is symplectic and conserves the energy up to the round-off error [40]. For each particle, time integration is carried out until the particle has completely left the RD. Numerically, this is well verified when $|x(t)| > 3|x_0|/2$.

IV. RESULTS

To quantify how the pitch-angle cosine is modified in a population of particles because of their interaction with a RD, we define a regular 2D grid $\{w_{0;i}, \phi_{0;j}\}$ in the (w_0, ϕ_0) plane, formed by $N_w \times N_\phi$ points: $w_{0;i} = i\,\delta w$, $\phi_{0;j} = j\,\delta\phi$, with $i = 1, \ldots, N_w$, $j = 0, \ldots, N_\phi - 1$, and $\delta w = 1/N_w$, $\delta\phi = 2\pi/N_\phi$. Such grid points determine a set of initial conditions for an equal number of particles. For all particles we have solved the motion equations (2) until calculating the final pitch-angle cosine $w_{1;i,j}$ and the corresponding variation $\Delta w_{i,j} = w_{1;i,j} - w_{0;i}$. The distribution of the pitch-angle cosine variation $f(\Delta w_{i,j})$ has been calculated, and this procedure has been repeated for different values of the parameters α and β. We notice that $0 < w_{0;i} \leqslant 1$, in order to have $v_{||} > 0$ at the initial time, while $-1 \leqslant w_{1;i,j} \leqslant 1$. Therefore $\Delta w_{i,j}$ varies in the range $-2 \leqslant \Delta w_{i,j} < 1$. In Fig. 5 the distribution $f(\Delta w_{i,j})$ is plotted as a function of $\Delta w_{i,j}$ for various values of the rotation angle β and for $\alpha = 45^\circ$. In this figure we have set $N_w = N_\phi = 10^3$. For $\beta = 15^\circ$ the distribution is centered around $\Delta w_{i,j} = 0$ and has a relatively small width; in particular, a sharp peak is present at $\Delta w_{i,j} \simeq 0$. In this case, particles crossing the RD have small but finite variations of the pitch-angle cosine. The behavior of $f(\Delta w_{i,j})$ in the small interval $15^\circ \leqslant \beta \leqslant 22^\circ$ is plotted in the inset of Fig. 5: A small increase in the rotation angle β results in the sharp peak rapidly flattening and splitting into two distinct peaks. Further increasing the rotation angle β, the width of the distribution function increases indicating the presence of particles whose final value w_1 is very different from w_0. In particular, for $\beta = 90^\circ$ the distribution extends over the whole range of $\Delta w_{i,j}$, and a population with $\Delta w_{i,j} \sim -2$ is visible, corresponding to the largest possible variation $|\Delta w_{i,j}|$. This behavior is consistent with what expected from Fig. 3: Increasing β corresponds

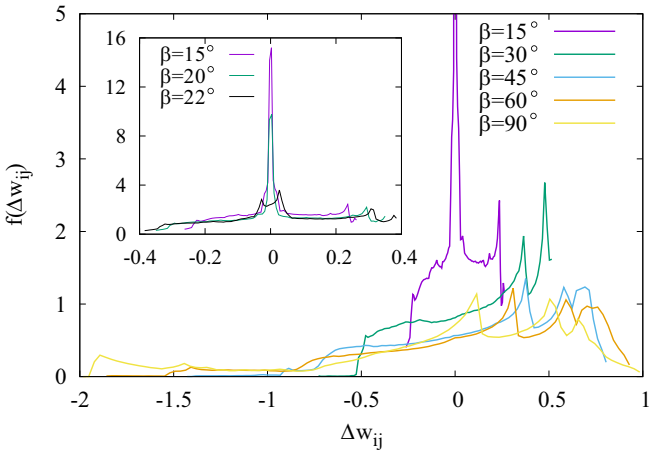

FIG. 5. The distribution $f(\Delta w_{i,j})$ of the pitch-angle cosine variation is plotted as a function of $\Delta w_{i,j}$, for $\alpha = 45^\circ$ and $\beta = 15^\circ$ (purple line), $\beta = 30^\circ$ (green line), $\beta = 45^\circ$ (light blue line), $\beta = 60^\circ$ (orange line), and $\beta = 90^\circ$ (yellow line); inset: $\alpha = 45^\circ$ and $\beta = 15^\circ$ (purple line), $\beta = 20^\circ$ (green line), $\beta = 22^\circ$ (black line).

to decreasing the curvature radius, leading to a progressive violation of magnetic momentum conservation. Summarizing, the scattering power of a RD on a population of particles increases with increasing the rotation angle β of **B** across the discontinuity. A certain amount of scattering is present even at small values of β, while large β values give rise to strong scattering in a single interaction with the RD.

In Fig. 6 2D maps of the final value w_1 are plotted as functions of the initial pitch-angle cosine w_0 and gyrophase ϕ_0, in the cases $\alpha = 45^\circ$, and $\beta = 15^\circ$, $\beta = 45^\circ$, $\beta = 90^\circ$. Lighter (darker) grey corresponds to positive (negative) w_1; the purple line is the contour separating regions where $w_1 > 0$ from regions where $w_1 < 0$. For small values of the rotation angle β (upper panel) the final pitch angle cosine remains always positive—except for initial pitch angles very close to 90°—indicating that almost no particles are reflected back by the RD. When increasing β, larger and larger regions in the $\{w_0, \phi_0\}$ plane appear where w_1 is negative, corresponding to reflected particles (middle and lower panels). We notice that for initial pitch angles close to 90°, the two regions where w_1 has opposite signs are strongly intermixed. This indicates that small variations in the initial parameters w_0, ϕ_0 can result in much larger variations of the final pitch-angle cosine w_1. For larger values of w_0 (i.e., particles with a large parallel velocity) the two regions are apparently more clearly separated. However, negative values of w_1 are found *even for large values* of the initial pitch-angle cosine: $w_0 \simeq 0.8$ (corresponding to $\theta_0 \simeq 37^\circ$) at $\beta = 45^\circ$ and $w_0 \simeq 1$ at $\beta = 90^\circ$. Therefore, a population of particles initially moving at small angles with **B** is reflected back by the RD; this property is more evident for large values of the rotation angle β.

Further details of the dependence of the final pitch-angle cosine w_1 on the initial condition can be observed in Fig. 7, where "cuts" of $w_1 = w_1(w_0, \phi_0)$ are plotted for a fixed value $w_0 = \cos 80^\circ \simeq 0.17$, as functions of ϕ_0 (red line in the middle panel of Fig. 6), in the case $\alpha = 45^\circ$, $\beta = 45^\circ$. In Fig. 7(a) the whole range $0 \leqslant \phi_0 \leqslant 360^\circ$ is represented. In most of this

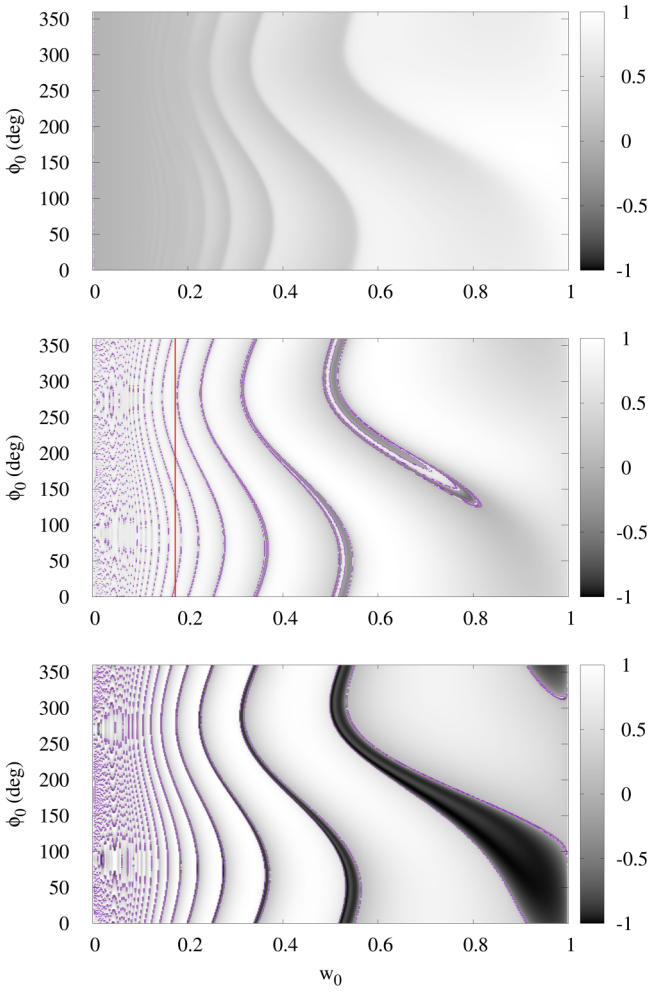

FIG. 6. Two-dimensional maps of the final value w_1 are plotted as functions of the initial pitch-angle cosine w_0 and gyrophase ϕ_0, for $\alpha = 45^\circ$ and $\beta = 15^\circ$ (upper panel), $\beta = 45^\circ$ (middle panel), $\beta = 90^\circ$ (lower panel). The purple line is the contour separating regions where $w_1 > 0$ from regions where $w_1 < 0$. The vertical red line in the middle panel indicates the location of the "cuts" plotted in Fig. 7.

range it is $w_1 > 0$, corresponding to forward-moving particles, and w_1 has a smooth dependence of the initial angle ϕ_0. However, some subranges are present where w_1, as a function of ϕ_0, shows very fast variations and can take negative values, corresponding to back-reflected particles. A blow-up of one of these subranges is represented in Fig. 7(b) [indicated by two vertical green lines in Fig. 7(a)], where a structure similar as in Fig. 7(a) is visible at a smaller scale; namely a succession of subdomains where $w_1(\phi_0)$ has either a smooth or a rapidly changing behavior. Further progressive enlargements of such subdomains plotted in Figs. 7(c) and 7(d) display the same behavior at increasingly smaller scale. Two properties can be infererred from Fig. 7: (i) Around regions of the (w_0, ϕ_0) plane where the final pitch-angle cosine w_1 is negative, w_1 is extremely sensitive to the initial condition, since very small variations of ϕ_0 and w_0 lead to very different final values w_1; this kind of behavior is typical of a chaotic dynamics. (ii) The line in the (w_0, ϕ_0) plane separating regions where

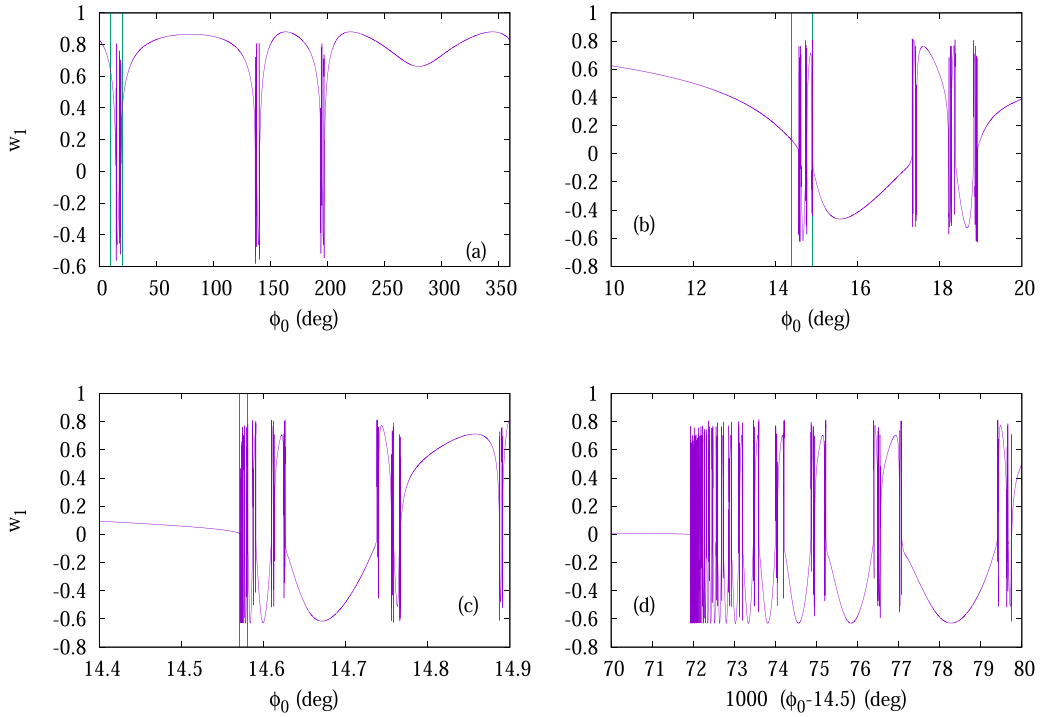

FIG. 7. The final pitch-angle cosine w_1 is plotted as a function of the initial gyrophase ϕ_0 for $w_0 = \cos 80^\circ \simeq 0.17$ in the case $\alpha = 45^\circ$, $\beta = 45^\circ$ (purple curves). Plot (a) refers to the whole range $0 \leqslant \phi_0 \leqslant 360^\circ$; plots (b) to (d) refer to increasingly small subintervals. Vertical green lines in plots (a) to (c) indicate the subinterval represented in the subsequent plot.

$w_1 < 0$ from those where $w_1 > 0$ appears to have self-similar properties and then could be a fractal. These two properties will be investigated in more details in the following.

In order to better show such a chaotic dynamics, in Fig. 8 the trajectories of two particles are plotted (upper panels) for the configuration $\alpha = \beta = 45^\circ$. These particles start with the

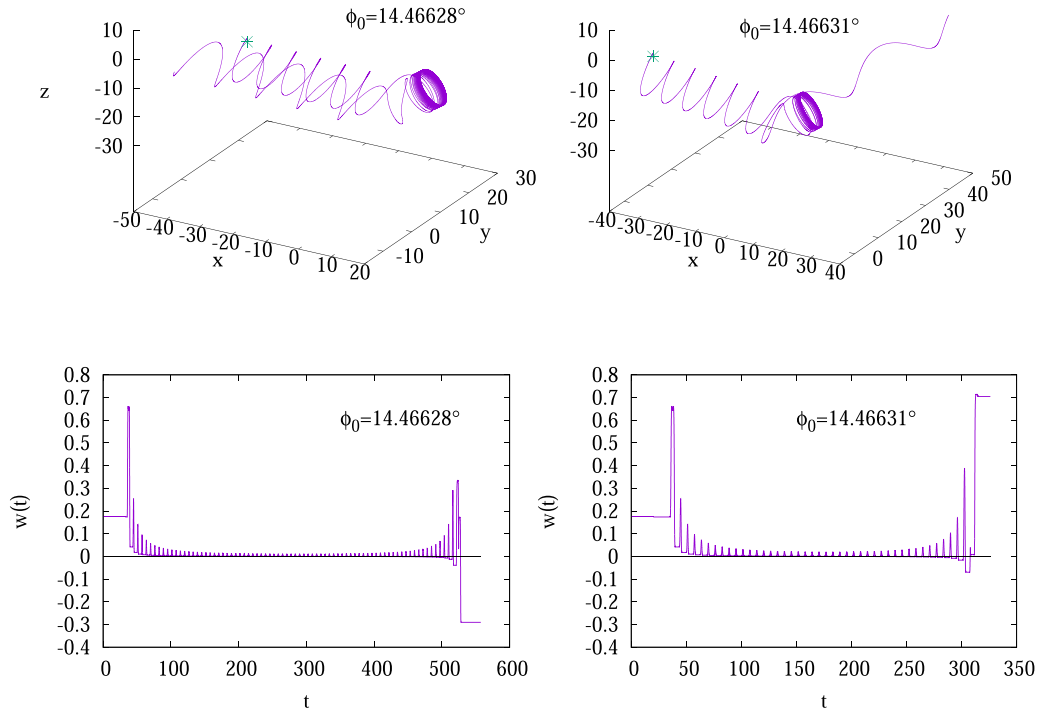

FIG. 8. Upper panels: The trajectories of two particles starting with two slightly different gyrophases $\phi_0 = 14.46628^\circ$ (left) and $\phi_0 = 14.46631^\circ$ (right) and with the same pitch angle $\theta_0 = 80^\circ$, in the configuration $\alpha = \beta = 45^\circ$; the green asterisk indicates the initial position. Lower panels: The pitch-angle cosine $w(t)$ is plotted as a function of time t for both particles.

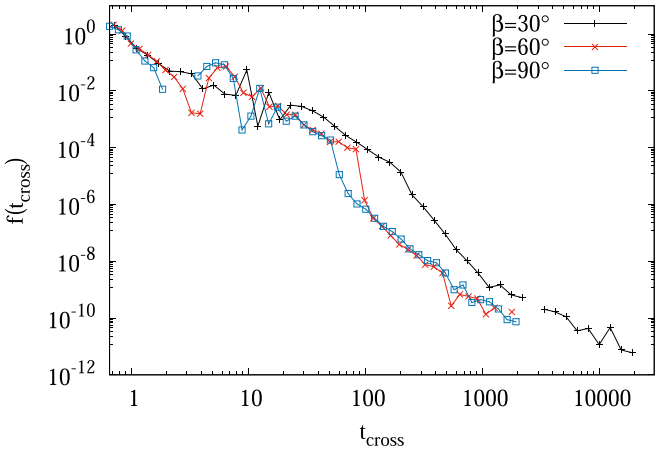

FIG. 9. The distribution f of particle crossing times $t_{\rm cross}$ is plotted in the cases $\alpha = 45^\circ$ and $\beta = 30^\circ$ (black line), $\beta = 60^\circ$ (red line), and $\beta = 90^\circ$ (blue line).

same pitch angle $\theta_0 = 80^\circ$ and with two almost equal gyrophases, the gyrophase difference being $\Delta\phi_0 = (3 \times 10^{-5})^\circ$. Left and right plots correspond to a particle that is reflected back (denoted by P1) and to a particle that goes beyond the RD (denoted by P2), respectively. When such particles approach the RD their pitch angle θ becomes close to 90° and particles remain "trapped" inside the RD for many gyroperiods. However, further interaction of the particles with the RD gradually modifies the dynamics and particles eventually leave the RD propagating either forward or backward. It can be noticed that a very small difference in the initial condition implies a completely different behavior, which is the hallmark of chaotic dynamics. Lower panels in Fig. 8 show how the pitch-angle cosine w varies in time and illustrate in more detail the trapping process. Trapping lasts for some hundreds of time units, corresponding to ∼80 or ∼43 gyroperiods for P1 or P2, respectively. At the beginning of the trapping stage, the pitch-angle cosine $w(t)$ follows a sequence of oscillations that damp approaching the value $w = 0$, with $w(t) > 0$. Of course, a consistently null w would correspond to an infinite trapping time. However, trapping is not stable and during a subsequent stage oscillations increase in amplitude, with $w(t)$ assuming also slightly negative values. Eventually, trapping ends and $w(t)$ rapidly reaches the final value w_1, either positive or negative.

The probability distributions of interaction times for an ensemble of 4×10^7 particles uniformly injected in the (w_0, ϕ_0) space are shown in Fig. 9 for three different values of β. It can be seen that these distributions are very broad, extending over more than three orders of magnitude: Very short times are found, comparable to or shorter than the gyrotime, confirming that RD can act as fast pitch-angle scatterers [24]. But also very long crossing times, which can be interpreted as the trapping times discussed above, are found with non-negligible probability; long time trapping is one of the properties of deterministic chaos and may have influence on the origin of anomalous transport [41,42]. The distributions of crossing times may roughly be described as power-law distributions with a slope of about -3. Some local oscillations can be seen around $t_{\rm cross} \sim 10$: These are not statistical fluctuations, since the statistical error is less than 10^{-3} times the reported values, and therefore they reflect the complexity of the chaotic dynamics. Also, a change of slope around $t_{\rm cross} \sim 100$ can be seen, which drifts to lower times for increasing β.

In order to further assess the chaotic properties of the particle dynamics in the (w_0, ϕ_0) space, we have characterized the line Γ_0 separating regions where $w_1 < 0$ (reflected particles) from those where $w_1 > 0$ (forward particles) (purple line in Fig. 6) by calculating its Hausdorff dimension D. For a regular curve one has $D = 1$, for a surface it is $D = 2$, while a fractal in the plane has an intermediate Hausdorff dimension $1 < D < 2$. The Hausdorff dimension of the curve Γ_0 has been calculating employing a box-counting method [43], as described in the following: (i) we calculated the final pitch-angle cosine on the above-defined gridpoints: $w_{1;i,j} = w_1(w_{0;i}, \phi_{0;j})$, thus obtaining $N_w \times N_\phi$ values, with $N_w = N_\phi = N = 2^{12} = 4096$. (ii) We selected gridpoints belonging to the line Γ_0 in the following way: A given gridpoint $(w_{0;i}, \phi_{0;j})$ is assumed to belong to Γ_0 if the sign of $w_{1;i,j}$ is different from the sign of $w_{1;i\pm1,j}$ or $w_{1;i,j\pm1}$, i.e., of w_1 calculated on at least one of the four next-neighbor points. (iii) We defined a hierarchy of $(\log_2 N) + 1$ partitions of the (w, ϕ) plane. Each partition is identified by the upper index (n), with $n = 0, \ldots, \log_2 N$. The (n)th partition is composed by a set of equal disjunct rectangular subdomains ("boxes") $D^{(n)}_{k,l} = \{(w_{0;i}, \phi_{0;j})\}$, with $(k-1)2^n + 1 \leqslant i < k2^n$, $(l-1)2^n + 1 \leqslant j < l2^n$, and $1 \leqslant k, l \leqslant N/2^n$. The size of boxes of the (n)th partition is $R_n = 2^n$. Each partition covers the entire (w_0, ϕ_0) plane; increasing the partition index by one unit: $n \to n+1$ multiplies the size R_n of boxes by a factor 2; in the lowest partition $n = 0$ all boxes $D^{(0)}_{k,l}$ are single gridpoints, while the highest partition $n = \log_2 N$ contains a single box which coincides with the whole (w_0, ϕ_0) plane. (iv) Finally, for each partition (n) we count the number N_n of boxes that contain at least one point of the curve Γ_0. If Γ_0 is a fractal, then $N_n = cR_n^{-D}$, with c a constant [43], or

$$\log N_n = -D \log R_n + \log c. \tag{7}$$

Therefore, the Hausdorff dimension D of Γ_0 can be calculated as the opposite of the angular coefficient of a linear dependence expressed by the relation (7).

In Fig. 10 (left panel) the number N_n of non empty boxes in the (n)th partition is plotted as a function of the box size R_n, for $\alpha = 45^\circ$ and $\beta = 30^\circ$ or $\beta = 90^\circ$. It is clear that the function relating N_n with R_n approximately follows a power law, whose index $-D$ can be determined by a fitting procedure. Power laws that fit data points are indicated by dashed lines. In the right panel of Fig. 10 the resulting Hausdorff dimension D is plotted as a function of the rotation angle β, in the interval $30^\circ \leqslant \beta \leqslant 90^\circ$ and for $\alpha = 45^\circ$. We see that in all the considered interval it is $D \simeq 1.64$, with D slightly varying with β. So we can say that for $\beta \geqslant 30^\circ$ the RD is consistently generating chaotic behavior and large pitch-angle scatterings. Since the Hausdorff dimension D is intermediate between 1 and 2, we conclude that the curve Γ_0 separating regions of the (w_0, ϕ_0) plane corresponding to $w_1 > 0$ from regions corresponding to $w_1 < 0$ is a fractal. In contrast, Γ_0 is a regular curve for smaller values β. We conclude that particles with a chaotic behavior and a fractal phase space

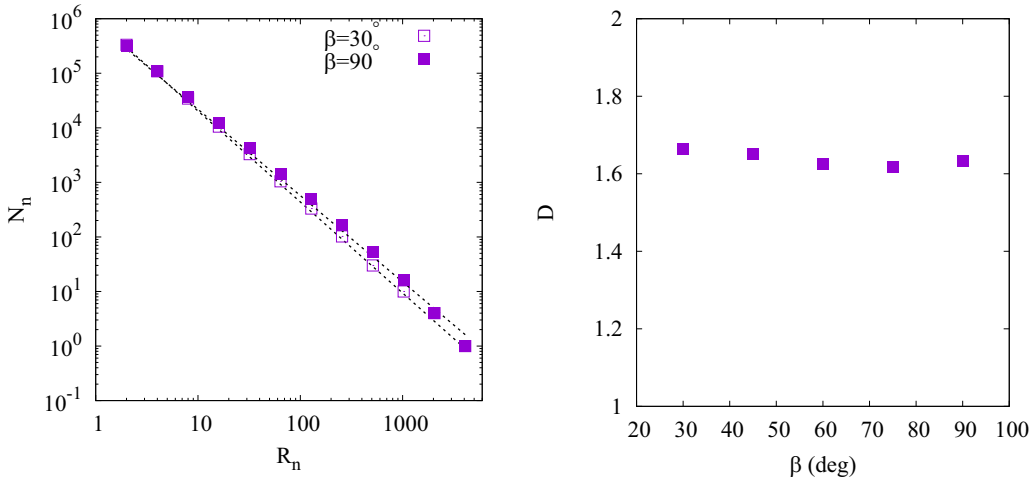

FIG. 10. Left: The number N_n of non empty boxes found in the (n)th partition (squares) and the fitting law (7) (dotted lines) are plotted as a function of the box size R_n, for $\beta = 30^\circ$ and $\beta = 90^\circ$. Right: The Hausdorff dimension D of the line Γ_0 resulting from the fitting procedure as a function of the rotation angle β.

are present in configurations where the curvature radius of magnetic lines is smaller than the Larmor radius (see Fig. 3).

V. DISCUSSIONS AND CONCLUSIONS

Motivated by the frequent observations of RDs and current sheets in space plasmas, we have studied the dynamics of charged particles interacting with an ideal MHD rotational discontinuity by means of a test particle simulation. The RD is described by an analytical model with constant magnetic field intensity, and field line rotation described by the angle β; also the direction of the magnetic field with respect to the normal-to-the-discontinuity direction is described by the angle α. By injecting particles with random initial velocity direction directed toward the RD, we can study the particle trajectories by means of a simplectic integrator.

We find that particles having the Larmor radius comparable to or larger than RD field line radius of curvature exhibit marked chaotic properties. In particular, the pitch-angle cosine w_1 of particles having interacted with the RD is only weakly related to the initial pitch-angle cosine w_0, and this relation vanishes for $\beta \to 90^\circ$ (see Fig. 5). This behavior is typical of chaotic dynamics and shows that RDs are very effective pitch-angle scatterers, a fact that should be taken into account in many astrophysical plasmas, in particular when considering cosmic ray propagation. Close analysis of the dependence of w_1 on ϕ_0 shows a high sensitivity and a self-similar hierarchy of values of ϕ_0 that can result in the full range of values of w_1 (see Fig. 7). In addition, energetic particles can be trapped for long times within the RD, and the crossing or trapping times have an approximately power-law distribution. The study of the initial positions in velocity space, quantified by (w_0, ϕ_0), which correspond to either crossing $(w_1 > 0)$ or reflected $(w_1 < 0)$ particles shows the emergence of a fractal structure, with a fractal dimension close to 1.63. This confirms the complexity of the underlying dynamics and the strong unpredictability of the results of RD-particle interaction. Our study complements those of Wilkinson [44], where the particle dynamics is studied analytically with the aim to understand the interaction with an ideal magnetic field structure associated with a collisionless shock wave, and of Artemyev *et al.* [24], where it is shown that fast ion pitch-angle scattering is related to the destruction of the longitudinal adiabatic invariant (the longitudinal direction being that parallel to $\mathbf{B}_n$). We note that while Wilkinson [44] finds that the space of initial conditions of pitch angle and gyrophase can be divided in relatively simple domains of particles either returning to or escaping upstream of the discontinuity (see Fig. 2 in Wilkinson [44]) we find that the domains corresponding to either crossing or noncrossing particles have indeed a fractal structure, see our Figures 6 and 10.

These results may have important implications for energetic particle scattering in space and astrophysical plasmas. Indeed, efficient pitch-angle scattering has a direct influence on energetic particle transport parallel to the magnetic field, given that the pitch angle determines the parallel velocity. In the case of pitch-angle scattering due to the resonant interaction with magnetic turbulence, the spatial diffusion coefficient is inversely proportional to the pitch-angle diffusion coefficient and a fast pitch-angle scattering leads to short acceleration times in the mechanisms of diffusive shock acceleration (DSA) [14,45]. We may argue that rotational discontinuities can effectively contribute to efficient pitch-angle scattering, and therefore contribute to decrease the acceleration times at shocks (which is one crucial problem for DSA [46]); however, a point that deserves further investigation is about the availability of a sufficient "supply" of RDs in the regions around shocks where acceleration is supposed to happen. In this connection, *in situ* observations in the solar wind and in the near-Earth environment have pointed out the presence of ubiquitous magnetic field discontinuities [19–21,25,47,48]. Further, Refs. [16,22] have shown that many discontinuities and current sheets are nested over a broad range of spatial/timescales in space plasmas: This suggests that fast pitch-angle scattering due to the associated RDs could be found on many spatial scales, corresponding to the Larmor radius of particles of different energies. These considerations lead us to the conclusion that pitch-angle scattering

due to RDs in astrophysical plasmas should be consistently taken into account.

We point out that our test-particle approach, although simplified, can be considered appropriate since the dynamic pressure of energetic particles is usually smaller than that of thermal particles. The present results have been obtained for a fixed velocity $v = 6$, corresponding to a gyroradius of the same order as the field line radius of curvature. For smaller velocities (smaller gyroradii) we can expect an adiabatic particle motion with negligible pitch-angle scattering, while for larger velocities (larger gyroradii) it is possible that the dynamics of the system will be chaotic for a broader range of values of the model parameters. Indeed, low-speed particles "see" the RD as a smooth rotation of the field lines, thus undergoing small pitch-angle scattering; conversely, high-speed particles interact with abruptly bending magnetic field lines, thus experiencing a large pitch-angle scattering which sensitively depends on the initial gyrophase. The study of the dependence on v is deferred to a future work.

An additional issue which deserves further investigations is related to the finding that particles may be trapped in the RD for both short and long times, or, in other words, that a power-law distribution of trapping times is found, see Fig. 9. In the field of anomalous diffusion, the latter property is the basis of subdiffusive behavior [41,42]. Again, a spatial subdiffusive behavior of energetic particles can lead to a decrease in the acceleration time of DSA [49], since particles trapped in, say, an RD in the solar wind upstream of a shock wave can be quickly convected into the shock and be accelerated. On the other hand, it is tempting to interpret the trapping times as long scattering times, since those are a basic ingredient in the non-Markovian transport model of [45]; however, caution is necessary on this point.

Finally, we note the our simple model does not take into account those more complex spatial structures and temporal fluctuations that are present in actual space and astrophysical plasmas. Therefore, our results could be modified by perturbations; for instance, these could smear out the fractal structure in the (w_0, ϕ_0) plane and possibly reduce the duration of particle trapping in the RD. However, many properties of chaotic systems are resilient to small perturbations, as indicated by the Kolmogorov-Arnold-Moser theorem, too. As an example, interesting clues come from studies of ion motion in the Earth's magnetotail: there, a different magnetic field configuration is found, usually modeled as a parabolic field reversal, which also is capable of generating chaotic motion [39] and resonant particle acceleration at discrete locations—the so-called beamlets [50]. In Ref. [51], it is shown by a numerical study that such resonant acceleration at discrete locations is also found when electromagnetic perturbations of small amplitude are introduced in the system. This supports the view that the results of simplified nonlinear models remain valid even in the presence of perturbations if the latter are not too strong.

[1] M. A. Lee, R. A. Mewaldt, and J. Giacalone, Shock acceleration of ions in the heliosphere, Space Sci. Rev. **173**, 247 (2012).

[2] W. H. Matthaeus, G. Qin, J. W. Bieber, and G. P. Zank, Nonlinear collisionless perpendicular diffusion of charged particles, Astrophys. J. Lett. **590**, L53 (2003).

[3] F. Pucci, F. Malara, S. Perri, G. Zimbardo, L. Sorriso-Valvo, and F. Valentini, Energetic particle transport in the presence of magnetic turbulence: Influence of spectral extension and intermittency, Mon. Not. R. Astron. Soc. **459**, 3395 (2016).

[4] J. A. Tessein, D. Ruffolo, W. H. Matthaeus, M. Wan, J. Giacalone, and M. Neugebauer, Effect of coherent structures on energetic particle intensity in the solar wind at 1 AU, Astrophys. J. **812**, 68 (2015).

[5] P. Veltri and A. Mangeney, Scaling laws and intermittent structures in solar wind MHD turbulence, in *Solar Wind Nine*, American Institute of Physics Conference Series, Vol. 471, edited by S. R. Habbal, R. Esser, J. V. Hollweg, and P. A. Isenberg (American Institute of Physics, College Park, MD, 1999), pp. 543–546.

[6] G. Zimbardo, A. Greco, L. Sorriso-Valvo, S. Perri, Z. Vörös, G. Aburjania, K. Chargazia, and O. Alexandrova, Magnetic turbulence in the geospace environment, Space Sci. Rev. **156**, 89 (2010).

[7] R. Bruno and V. Carbone, The solar wind as a turbulence laboratory, Liv. Rev. Sol. Phys. **10**, 2 (2013).

[8] J. R. Jokipii, Cosmic-ray propagation. I. Charged particles in a random magnetic field, Astrophys. J. **146**, 480 (1966).

[9] P. Pommois, G. Zimbardo, and P. Veltri, Energetic particle transport in anisotropic magnetic turbulence, Adv. Space Res. **35**, 647 (2005).

[10] M. Hussein and A. Shalchi, Simulations of energetic particles interacting with dynamical magnetic turbulence, Astrophys. J. **817**, 136 (2016).

[11] M. A. Lee and L. A. Fisk, Shock acceleration of energetic particles in the heliosphere, Space Sci. Rev. **32**, 205 (1982).

[12] N. U. Crooker, J. T. Gosling, V. Bothmer, R. J. Forsyth, P. R. Gazis, A. Hewish, T. S. Horbury, D. S. Intriligator, J. R. Jokipii, J. Kóta, A. J. Lazarus, M. A. Lee, E. Lucek, E. Marsch, A. Posner, I. G. Richardson, E. C. Roelof, J. M. Schmidt, G. L. Siscoe, B. T. Tsurutani *et al.*, CIR morphology, turbulence, discontinuities, and energetic particles, Space Sci. Rev. **89**, 179 (1999).

[13] J. Giacalone, Cosmic-ray transport and interaction with shocks, Space Sci. Rev. **176**, 73 (2013).

[14] E. Amato, The origin of galactic cosmic rays, Int. J. Mod. Phys. D **23**, 1430013 (2014).

[15] P. Wu, S. Perri, K. Osman, M. Wan, W. H. Matthaeus, M. A. Shay, M. L. Goldstein, H. Karimabadi, and S. Chapman, Intermittent heating in solar wind and kinetic simulations, Astrophys. J. Lett. **763**, L30 (2013).

[16] A. Greco and S. Perri, Identification of high shears and compressive discontinuities in the inner heliosphere, Astrophys. J. **784**, 163 (2014).

[17] S. Perri, S. Servidio, A. Vaivads, and F. Valentini, Numerical study on the validity of the taylor hypothesis in space plasmas, Astrophys. J. Suppl. Ser. **231**, 4 (2017).
[18] D. Perrone, R. Bruno, R. D'Amicis, D. Telloni, R. De Marco, M. Stangalini, S. Perri, O. Pezzi, O. Alexandrova, and S. D. Bale, Coherent events at ion scales in the inner Heliosphere: Parker Solar Probe observations during the first Encounter, Astrophys. J. **905**, 142 (2020).
[19] B. T. Tsurutani and E. J. Smith, Interplanetary discontinuities: Temporal variations and the radial gradient from 1 to 8.5 AU, J. Geophys. Res. **84**, 2773 (1979).
[20] J. E. Borovsky, Contribution of Strong Discontinuities to the Power Spectrum of the Solar Wind, Phys. Rev. Lett. **105**, 111102 (2010).
[21] S. Perri, M. L. Goldstein, J. C. Dorelli, and F. Sahraoui, Detection of Small-Scale Structures in the Dissipation Regime of Solar-Wind Turbulence, Phys. Rev. Lett. **109**, 191101 (2012).
[22] A. Greco, S. Perri, S. Servidio, E. Yordanova, and P. Veltri, The complex structure of magnetic field discontinuities in the turbulent solar wind, Astrophys. J. Lett. **823**, L39 (2016).
[23] T. D. Phan, S. D. Bale, J. P. Eastwood, B. Lavraud, J. F. Drake, M. Oieroset, M. A. Shay, M. Pulupa, M. Stevens, R. J. MacDowall, A. W. Case, D. Larson, J. Kasper, P. Whittlesey, A. Szabo, K. E. Korreck, J. W. Bonnell, T. D. de Wit, K. Goetz, P. R. Harvey *et al.*, Parker solar probe in situ observations of magnetic reconnection exhausts during encounter 1, Astrophys. J. Supp. **246**, 34 (2020).
[24] A. V. Artemyev, A. I. Neishtadt, A. A. Vasiliev, V. Angelopoulos, A. A. Vinogradov, and L. M. Zelenyi, Superfast ion scattering by solar wind discontinuities, Phys. Rev. E **102**, 033201 (2020).
[25] R. Bruno, V. Carbone, P. Veltri, E. Pietropaolo, and B. Bavassano, Identifying intermittency events in the solar wind, Plan. Space Sci. **49**, 1201 (2001).
[26] L. F. Burlaga, Directional discontinuities in the interplanetary magnetic field, Solar Phys. **7**, 54 (1969).
[27] R. N. Martin, J. W. Belcher, and A. J. Lazarus, Observation and analysis of abrupt changes in the interplanetary plasma velocity and magnetic field, J. Geophys. Res. **78**, 3653 (1973).
[28] E. J. Smith, Identification of interplanetary tangential and rotational discontinuites., J. Geophys. Res. **78**, 2054 (1973).
[29] F. Mariani, B. Bavassano, and U. Villante, A statistical study of magnetohydrodynamic discontinuities in the inner solar system - HELIOS-1 and HELIOS-2, Solar Phys. **83**, 349 (1983).
[30] M. Neugebauer, The structure of rotational discontinuities, Geophys. Res. Lett. **16**, 1261 (1989).
[31] A. Soding, F. M. Neubauer, B. Tsurutani, N. F. Ness, and R. P. Lepping, Radial and latitudinal dependencies of discontinuities in the solar wind between 0.3 and 19 AU and -80° and $+10^\circ$, Ann. Geophys. **19**, 667 (2001).
[32] L. F. Burlaga and N. F. Ness, Tangential discontinuities in the solar wind, Solar Phys. **9**, 467 (1969).
[33] T. Horbury, D. Burgess, M. J. Fränz, and C. J. Owen, Three spacecraft observations of solar wind discontinuities, Geophys. Res. Lett. **28**, 677 (2001).
[34] T. Knetter, F. M. Neubauer, T. Horbury, and A. Balogh, Discontinuity observations with cluster, Adv. Space Res. **32**, 543 (2003).
[35] T. Knetter, F. M. Neubauer, T. Horbury, and A. Balogh, Four-point discontinuity observatiocns using Cluster magnetic field data: A statistical survey, J. Geophys. Res.: Space Phys. **109**, A06102 (2004).
[36] J. W. Belcher and L. Davis, Large-amplitude Alfvén waves in the interplanetary medium, 2, J. Geophys. Res. **76**, 3534 (1971).
[37] D. A. Roberts, Construction of Solar-Wind-Like Magnetic Fields, Phys. Rev. Lett. **109**, 231102 (2012).
[38] F. Valentini, F. Malara, L. Sorriso-Valvo, R. Bruno, and L. Primavera, Building up solar-wind-like 3D uniform-intensity magnetic fields, Astrophys. J. Lett. **881**, L5 (2019).
[39] J. Buechner and L. M. Zelenyi, Regular and chaotic charged particle motion in magnetotaillike field reversals. 1. Basic theory of trapped motion, J. Geophys. Res. **94**, 11821 (1989).
[40] S. D. Webb, Symplectic integration of magnetic systems, J. Comput. Phys. **270**, 570 (2014).
[41] R. Metzler and J. Klafter, The random walk's guide to anomalous diffusion: A fractional dynamics approach, Phys. Rep. **339**, 1 (2000).
[42] V. Zaburdaev, S. Denisov, and J. Klafter, Lévy walks, Rev. Mod. Phys. **87**, 483 (2015).
[43] B. Mandelbrot, *The Fractal Geometry of Nature* (W. H. Freeman & Company, New York, 1983).
[44] W. P. Wilkinson, Analytical study of gyrophase, pitch angle, and normal speed of particles leaving an ideal magnetohydrodynamic discontinuity surface, Phys. Rev. E **102**, 023211 (2020).
[45] G. Zimbardo and S. Perri, Non-markovian pitch-angle scattering as the origin of particle superdiffusion parallel to the magnetic field, Astrophys. J. **903**, 105 (2020).
[46] P. O. Lagage and C. J. Cesarsky, The maximum energy of cosmic rays accelerated by supernova shocks, Astron. Astrophys. **125**, 249 (1983).
[47] B. T. Tsurutani, C. M. Ho, E. J. Smith, M. Neugebauer, B. E. Goldstein, J. S. Mok, J. K. Arballo, A. Balogh, D. J. Southwood, and W. C. Feldman, The relationship between interplanetary discontinuities and Alfvén waves: Ulysses observations, Geophys. Res. Lett. **21**, 2267 (1994).
[48] J. E. Borovsky, Flux tube texture of the solar wind: Strands of the magnetic carpet at 1 AU? J. Geophys. Res. **113**, A08110 (2008).
[49] P. Duffy, J. G. Kirk, Y. A. Gallant, and R. O. Dendy, Anomalous transport and particle acceleration at shocks, Astron. Astrophys. **302**, L21 (1995).
[50] M. Ashour-Abdalla, L. A. Frank, W. R. Paterson, V. Peroomian, and L. M. Zelenyi, Proton velocity distributions in the magnetotail: Theory and observations, J. Geophys. Res. **101**, 2587 (1996).
[51] M. S. Dolgonosov, G. Zimbardo, S. Perri, and A. Greco, On the generation of ion beamlets in the magnetotail: Resonant acceleration versus stochastic acceleration, J. Geophys. Res. (Space Phys.) **118**, 5445 (2013).